Feasibility Study of Frequency-difference Electrical Impedance Tomography on Industrial Applications

Feasibility Study of Frequency-difference Electrical Impedance Tomography on Industrial Applications

Hancong Wu, Yunjie Yang, Javier Escudero, Jiabin Jia

Agile Tomography Group, School of Engineering, University of Edinburgh
The Kings Buildings, The Univerisity of Edinburgh, EH9 3JL, Edinburgh, UK
jiabin.jia@ed.ac.uk

ABSTRACT

The common working procedure of Electrical Impedance Tomography (EIT) needs to take a reference measurement when the phantom is full of homogenous continuous phase, like water. However, in practical industrial operations, the conductivity of continuous phase always varies due to the effects of the changes of ambient and fluid temperature, ionic concentration, and internal energy conversion in a fluid. Sometimes it is impracticable for practical process to have a homogenous continuous phase in the phantom for the purpose of taking a new reference for EIT. In order to overcome the difficulties raised by the traditional EIT in industrial applications, the frequency-difference EIT (fdEIT) adopted in medical applications could be an alternative solution for this problem. In this approach, the characteristics difference of multiple materials at two different frequencies is used to reconstruct the tomographic image. In this paper, the principle of fdEIT is explained in the finite element simulation. The method of selecting two optimal frequencies is studied and the performance of fdEIT is verified on the experimental rig. The limitation of our system and the future improvements are discussed.

Keywords EIT, frequency-difference, frequency selection, industrial applications

1 INTRODUCTION

Electrical Impedance Tomography (EIT) is an imaging technique which can infer images of electrical conductivity and permittivity of objects from surface electrode measurements (Holder 2004). In EIT, electric currents are injected into the object with a certain pattern through peripheral electrodes and the boundary voltages are measured (Harikumar 2013). Based on a reconstruction algorithm, the boundary voltages data are used to reconstruct images of the conductivity distribution inside the imaging object (Polydorides 2002, Harikumar 2013).

So far, time-difference EIT (tdEIT) is applied to various industrial operations as a real-time monitoring method (Wang 2001, Stanley 2005, Rodgers 2010) because of the high temporal resolution of EIT. In tdEIT, two measurements are executed at different times: the first one is taken as a reference when the EIT sensor is full of homogenous conductive liquid and the second one is taken when the dispersed phase is introduced into the sensor. The change in conductivity distribution between two measurements is computed and displayed on the images (Jun 2009). With a constant ambient temperature and time-invariant materials, common errors such as background noise and sensor geometrical errors are effectively cancelled out by subtracting data of two sets of data. However, in practical industrial operations, the situation of homogenous conductive liquid cannot always be provided for EIT to take a reference measurement, which causes problems for tdEIT's industrial applications.

To solve this problem, the medical researchers tried to measure the voltage component between different frequencies instead of time (Lee 2012, Packham 2012), which is frequency-difference EIT (fdEIT). Unlike tdEIT, measurement data for stimulation current in different frequencies can be obtained simultaneously so that initial reference is no longer needed. As frequency-dependent behaviours of different materials vary, their conductivities under different frequencies are discrepant (Castro-Giráldez 2010). By reconstructing the image of conductivity change between two frequencies, one material can be distinguished from others through its unique frequency dependent behaviours

(Seo 2008). The larger difference between two materials under selected frequencies results in the higher contrast between them in the reconstructed images. Therefore, how to select the optimal stimulation frequencies is imperative for image quality.

In this paper, EIT image reconstruction based on frequency-difference is investigated. The theories of fdEIT are introduced, followed by the analysis of conductivity change in the same material between frequencies. Non-iterative Tikhonov regularization with Laplacian of Gaussian (LoG) operator (Yang 2014) is selected for the inverse algorithm and the advantages of this algorithm are explained. To improve the quality of reconstructed images, a frequency selection algorithm is proposed to optimize the stimulation frequencies based on the frequency-dependent behaviours of materials. Industrial manufacture, such as food industry (Downing 2013), may adopt our method for real-time monitoring and reduction of defects.

2 METHODOLOGY

2.1 fdEIT Forward Problem and Weighted Boundary Voltage Calculation

EIT is a process that represents the electrical properties on an image from the voltages measured on the boundary of sensing domain (Polydorides 2002). It can be described by the equation:

$$\delta V = S\delta\sigma \tag{1}$$

where δV is the voltage difference matrix, $\delta\sigma$ is the conductivity difference matrix and S is the sensitivity matrix.

In fdEIT, δV and $\delta\sigma$ indicate the difference in the boundary voltages and the conductivity change within the model between two stimulation frequencies. *S* is the sensitivity matrix. Using finite element method, the model can be separated into pixels and the conductivity within one pixel is assumed to be constant. Derived from the Maxwell's equations, the complex conductivity of each pixel σ_V can be described by its conductivity σ_S and relative permittivity $\boldsymbol{\varepsilon}$ (Wiak 2008):

$$\sigma_V = \sigma_S + j\omega\varepsilon_0\varepsilon \tag{2}$$

If a material within the pixel does not have frequency-dependent behaviour, conductivity σ_S and permittivity ε are fixed regardless with frequency in equation (2). Therefore, the change of complex conductivity in terms of frequency is only related to the stimulation frequencies and relative permittivity:

$$\delta\sigma_V = j(\omega_2 - \omega_1)\varepsilon_0\varepsilon \tag{3}$$

where $\omega_1$and ω_2 are the stimulation angular frequencies at two sets of measurements and ε_0 is the permittivity of vacuum.

If conductivity σ_S has dependence on frequency (Kaewrawang 2007), complex conductivity difference between two frequencies can be written as:

$$\delta\sigma_V = (\sigma_{S2} - \sigma_{S1}) + j\varepsilon_0(\omega_2\varepsilon_2 - \omega_1\varepsilon_1) \tag{4}$$

The real part of the change of complex conductivity is not zero any more. At certain frequency range, the materials present unique conduction properties, which results in different complex conductivity change in different pixels, so that different materials can be distinguished from each other on the reconstructed images. Because the value of the imaginary part of the complex conductivity is much smaller than the real part, its effect to the images is ignored in this paper.

The complex conductivity in all pixels will be derived based on the boundary voltage vectors V_1 and V_2, which are measured in different frequencies. The boundary voltage vector δV is calculated by a weighted voltage difference method which can reduce the common modelling errors (Jun 2009). Its normalization form is denoted as:

$$\delta V = (V_2 - \alpha V_1)/\alpha V_1 \tag{5}$$

where α is a weight which equals to the inner product ratio between two voltages vectors:

$$\alpha = < V_2, V_1 > / < V_1, V_1 > \tag{6}$$

The boundary voltage vector δV is then used in the inverse problem of fdEIT to reconstruct the change in conductivity as shown in section 2.2.

2.2 Non-iterative Image Reconstruction

With known boundary voltage vector δV and sensitivity matrix S, computing the conductivity difference vector $\delta\sigma$ is to solve an inverse problem. The inverse problem of fdEIT is ill-posed, which means that equation (1) is ill-conditioned and the conductivity within the object cannot be resolved from the boundary voltage directly. The solution is to replace the original problem with a similar one but less ill-posed (Polydorides 2002). In real-time monitoring techniques, shorter image computing time per frame is preferred and non-iterative algorithms are used in this paper. Tikhonov regularization is one of the commonly used methods to solve ill-posed inverse problems and it can be expressed as (Yang 2003):

$$\delta\sigma = (S^T S + \mu E)^{-1} S^T \delta V \tag{7}$$

where μ is the regularization parameter and the identity matrix E is used to make the matrix $S^T S + \mu E$ invertible.

In applications where boundaries of different materials are obvious, the LoG (Sharifi 2002) can be utilised to sharpen the edges of the object. By replacing the identity matrix with the LoG operator matrix, which is constructed by the discrete approximation of Laplacian filter as shown in (8), the sharp edges between different materials can be precisely positioned and the calculation of conductivity change in each pixel within the model is more accurate.

$$\begin{bmatrix} 0 & -1 & 0 \\ -1 & 4 & -1 \\ 0 & -1 & 0 \end{bmatrix} \tag{8}$$

2.3 Frequency Selection Algorithm

The frequency-dependent behaviours of different materials do not always appear in the same frequency range (Nahvi 2008). The background noise under different frequencies is different as well. Selecting stimulation frequencies randomly for fdEIT may lead to either loss of information for material identification or low quality of the reconstructed images due to the large measuring errors. To reflect all the frequency-dependent behaviours in the reconstructed images without introducing large measuring errors, a frequency selection algorithm is a relevant option. Assume that the boundaries between different materials are close and clear, the number of objects appearing on the reconstructed image is proportional to the types of materials showing obvious frequency-dependent behaviours, which are less affected by the measuring errors, under selected frequencies. Using the frequencies where a maximum number of objects can be detected in the previous test in fdEIT measurements, different materials are much easier to be distinguished and reconstructed images with higher quality can be obtained.

A comprehensive contrast judgement algorithm, which bases on the mean of pixel values, is added to review the selecting frequencies and pick out the best pair of them. The comprehensive contrast value *M* in Figure 1 is related to the relative image error. When error is small, the comprehensive contrast value will be large. All pixels within the model are classified into background or anomalies. The average change in complex conductivity of background is calculated and it is used to determine the contrast between anomalies and background. The comprehensive contrast, which equals to the standard deviation of the contrast of each anomaly pixels, is used to estimate the flow of the algorithm is shown in Figure 1.

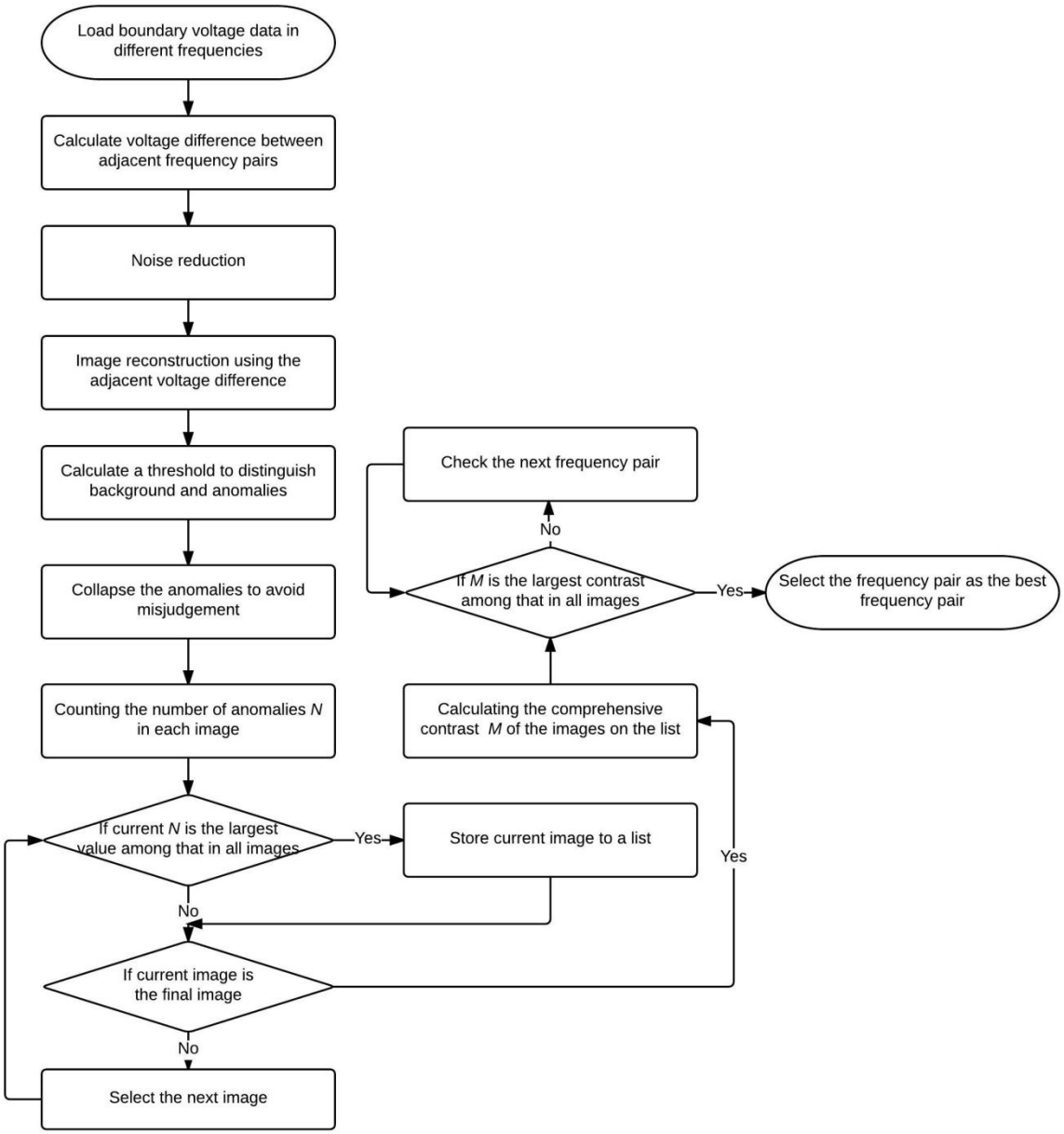

Figure 1. Process of frequency selection algorithm

2.4 Impedance Spectroscopy of Materials

Impedance spectroscopies of a potato sample and a sweet potato sample were scanned using the Keysight E4990A Impedance Analyser to estimate their conductivities change with frequency. Two samples were prepared to maintain the identical shape and volume. Their impedance magnitudes are shown in Figure 2(a). Referring to the general definition, the conductivity is the reciprocal of electrical resistivity and its relationship with impedance we measured can be represented by equation (8). The parameter *K* of both samples is the same, because of the identical shape and volume of two samples. Their conductivity change against frequency is shown in Figure 2(b) with the parameter *K*.

$$\sigma = K/Z \tag{8}$$

where σ is the complex conductivity of material, K is a factor related to the length and cross-sectional area of the sample and Z is the impedance. It is evident that the conductivity gradient of potato is larger than that of sweet potato.

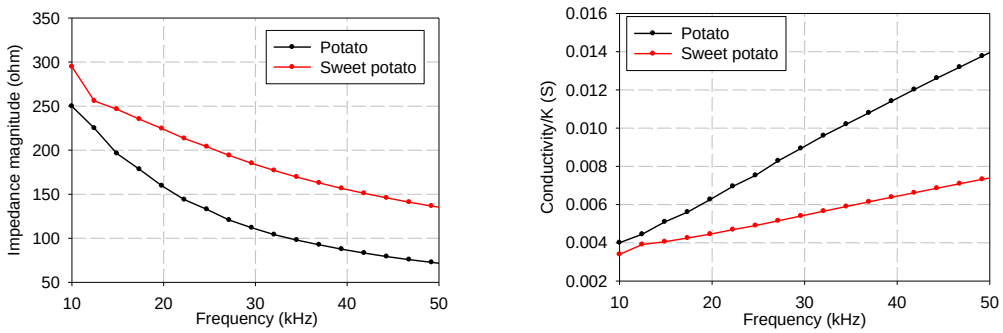

(a) (b)

Figure 2. (a) Impedance of potato and sweet potato against frequency, (b) Conductivity of potato and sweet potato against frequency

3 RESULTS AND DISCUSSION

3.1 Numerical Simulation

A simulation was performed using COMSOL and MATLAB. A two-dimension (2D) phantom (4.7 cm in diameter) was constructed in COMSOL with 16 electrodes equally spaced around its circumference. Inside the phantom, four circular anomalies with the same diameter were added into the phantom. They were aluminium, quartz and two virtual objects whose conductivities depended on frequency. Water was the background continuous material. Table 1 shows the conductivity and relative permittivity of these materials at frequencies from 10 kHz to 50 kHz. The red numbers in Table 1 indicate that the electrical conductivity of material 1 and material 2 is dependent on frequency.

In the simulations, five stimulation frequencies from 10 kHz to 50 kHz with 10 kHz interval were applied to the electrodes successively and the responding boundary voltages were recorded. White Gaussian Noise was added to the stimulated data to achieve a SNR of 80dB. To obtain a sensitivity map, the forward problem was solved numerically using the shape of the phantom. Frequency-difference images were reconstructed using the non-iterative image reconstruction algorithm mentioned in Section 2.1 based on the weighted voltage differences.

Table 1. Conductivity and relative permittivity of five different materials used in the numerical simulation

	Conductivity value in S/m; permittivity of vacuum = 8.85×10^{-12} F/m									
Frequency	Water (B)		Material 1 (C)		Aluminum (D)		Material 2 (E)		Quartz (F)	
	σ_S	ε	σ_S	ε	σ_S	ε	σ_S	ε	σ_S	ε
10 kHz	0.03	80	0.1	5000	5000	1	0.2	5000	1e-14	4.2
20 kHz	0.03	80	0.4	5000	5000	1	0.3	5000	1e-14	4.2
30 kHz	0.03	80	0.6	5000	5000	1	0.5	5000	1e-14	4.2
40 kHz	0.03	80	0.67	5000	5000	1	0.7	5000	1e-14	4.2
50 kHz	0.03	80	0.7	5000	5000	1	1	5000	1e-14	4.2

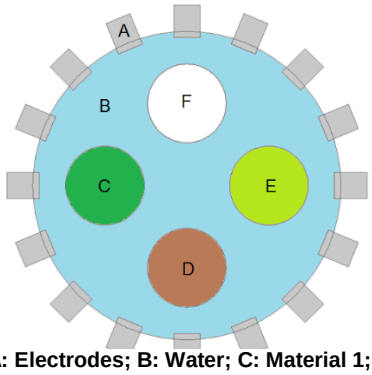

Figure 3. Setup in numerical simulation (A: Electrodes; B: Water; C: Material 1; D: Aluminium; E: Material 2; F: Quartz)

3.2 Numerical Simulation Results

Under the background of water, fdEIT was used to show the change in complex conductivities of aluminium, quartz, Material 1 and Material 2. For the purpose of comparison, all the anomalies were placed in the phantom symmetrically and simultaneously (Figure 3). Weighted frequency difference approach produced reconstructed images which reflected the relative conductivity changes of anomalies between frequencies (Figure 4).

According to Table 1, the electrical conductivities of aluminium and quartz was frequency independent, so their changes in complex conductivity against frequency should be calculated by equation (3). Since their relative permittivity was small, their complex conductivities almost remained constant at each stimulation frequency, which was similar to the complex conductivity of water. Therefore, none of them can be revealed from the background in the images in Figure 4 even though there was a large difference in their absolute conductivities. The conductivity of anomalies C and E in Figure 3 depended on stimulation frequencies. Their change in complex conductivity against frequency was much higher than that of water, so they can be distinguished in the reconstructed images. In stimulation frequency between 10 kHz and 20 kHz, the conductivity change of Material 1 (0.3 S/m) was higher than that of Material 2 (0.1 S/m). As a result, anomaly C constructed by Material 1 was more obvious in the reconstructed image under this frequency range (Figure 4 (a)) than anomaly E which was constructed by Material 2. In stimulation frequency between 30 kHz and 50 kHz, the ratio of conductivity change of Material 1 (0.1 S/m) kept decreasing and it was lower than that of Material 2 (0.5 S/m), so anomaly E was more observable in Figure 4 (b), (c) and (d).

It was noticeable that the conductivity change of both Material 1 and Material 2 was 0.2 S/m between 20 kHz and 30 kHz stimulation frequencies, but their contrasts to the background were different in Figure 4 (b). The reason of it should refer to the normalization process. In equation (5), the boundary voltage vector obtained was the voltage ratio between two stimulation frequencies instead of absolute value. Therefore, the conductivity vector we reconstructed in equation (7) can only reflect the ratio between conductivity in two frequencies. Although the absolute conductivity change of these two materials was the same, their conductivity difference in the starting frequency determined that they had a different ratio of the change in electric conductivity. Hence, anomaly C and anomaly E can be distinguished from each other on the image.

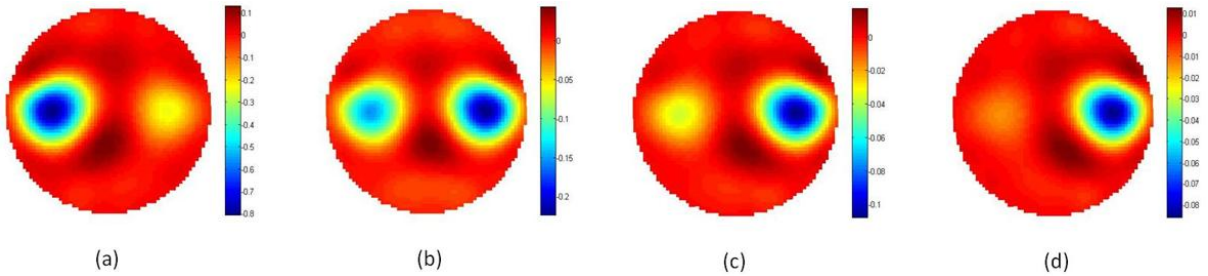

Figure 4. Reconstructed images for the numerical simulations under (a) 10 kHz and 20 kHz; (b) 20 kHz and 30 kHz; (c) 30 kHz and 40 kHz; (d) 40 kHz and 50 kHz

3.3 Verification Experiment

A plastic cylindrical vessel with 4.7 cm diameter, 7 cm height and 16 equally spaced stainless steel electrodes around its circumference was used in the experiment. Tap water was filled in the vessel until the electrodes were totally immersed. The conductivity of tap water was 0.02 S/m measured by the SensION+EC5 conductivity meter. The cylindrical potato sample and the cylindrical sweet potato sample were placed in the vessel as anomalies.

At room temperature, measurements were taken using an in-house developed multi-frequency EIT system. The stimulation current setting was the same as that in simulation and five sets of boundary voltages data were collected between 10 kHz and 50 kHz with 10 kHz interval. To test the performance of frequency selection algorithm, the connection between an electrode and the EIT system was modified to create an asymmetric error on purpose.

3.4 Verification of Experiment Results

Images were reconstructed from the experiment data using the same methods as those in simulations (Figure 5). Since there is a problem in the electrode, the background noise was large, causing special errors in the reconstructed images. In lower frequencies, the signal to noise ratio (SNR) of the EIT system was relatively low in comparison with that in higher frequencies. The deformation and displacement of the anomalies in lower frequencies were so large that two anomalies seemed to be merged with each other in the images of Figure 5 (b) and (c). In higher frequencies, the background noise reduced rapidly, allowing the images to reflect the conductivity changes of anomalies. In the images of Figure 5 (d) and (e), the potato was more evident than the sweet potato.

The frequency selection program was tested by using it to select the best frequency pair for these images. The number of anomalies which can be distinguished on the reconstructed image is compared with the expected number (2 in this case). Figure 5 (b) and (c) with large background noise were ruled out, since the number of anomalies detected is 1 as shown in Table 2. Then based on the comprehensive contrast calculated using the method described in Section 2.3, 30 kHz and 40 kHz with larger comprehensive contrast is selected as the best frequency pair for fdEIT among four options, which is the same as our selection by observation.

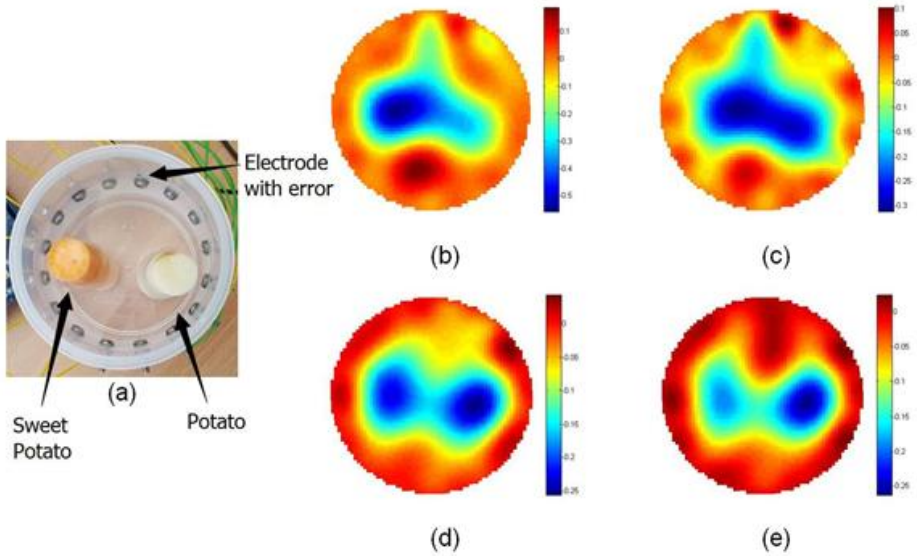

Figure 5. Experiment setup (a) and reconstructed images under (b) 10 kHz and 20 kHz; (c) 20 kHz and 30 kHz; (d) 30 kHz and 40 kHz; (e) 40 kHz and 50 kHz

Table 2. Resolution estimation result

Image number	Anomalies detected	Comprehensive contrast
Fig. 5 (b)	1	0.2083
Fig. 5 (c)	1	0.1132
Fig. 5 (d)	2	0.0797

Fig. 5 (e)	2	0.0566

3.5 Discussion

Basically, the simulation and experiment results are close to our expectation. In this paper, only 10 kHz intervals are analysed here, because we aims at selecting a best frequency pair when the interval is fixed. The conductivity change at two stimulation frequencies can be reflected on the images directly to display the anomalies. Materials whose electrical conductivity is independent to frequency have a small change in its complex permittivity between two stimulation frequencies, which makes them hard to be distinguished from the background. As a result, aluminium and quartz cannot be reconstructed in the images. The frequency selection algorithm successfully chooses the best frequency pair in our experiment, but it can only be applied to cases where the boundary between anomalies and background is clear. The blurred boundary may cause errors in the object counter, resulting in erroneous judgments for the selection of the best frequency pair. Although it cannot be used in medical imaging yet where the anatomical structure is much more complicated, it will improve the performance of fdEIT in some industrial applications, such as in food industry (Downing 2013), by optimal the stimulation frequencies.

4 CONCLUSION

Compared with time-difference EIT (tdEIT) imaging, frequency-difference EIT (fdEIT) does not require reference data, which allows its application to some industrial processes where homogenous and continuous phase cannot be accessed easily. With the help of frequency selection algorithm, fdEIT is able to reconstruct objects in a relatively high resolution and its operational cost is low. Both simulation and experiment work demonstrated the features of fdEIT. In future study, we will keep improving the frequency selection algorithm. Noise level might be measured to estimate the quality of an image, which is better than using comprehensive contrast. Frequencies up to 1 MHz cause low noise level in the system should all be taken into account so that images using multiple stimulation frequencies can be reconstructed and more information about the process materials can be extracted.

REFERENCES

CASTRO-GIRALDEZ, M., BOTELLA, P., TOLDRA, F. and FITO, P. (2010), Low-frequency dielectric spectrum to determine pork meat quality, Innovative Food Science & Emerging Technologies 11(2): 376-386.

DOWNING, D. L. (2013), A complete course in canning and related processes: processing procedures for canned food products, Elsevier.

HARIKUMAR R., PRABU, R. AND RAGHAVAN, S. (2013), Electrical Impedance Tomography (EIT) and Its Medical Applications: A Review, International Journal of Soft Computing Engineering 3(4): 2231-2307.

HOLDER, D. S. (2004), Electrical impedance tomography: methods, history and applications, CRC Press.

JUN, S. C., KUEN J., LEE J., WOO E. J., HOLDER, D. and SEO, J. K. (2009), Frequency-difference EIT (fdEIT) using weighted difference and equivalent homogeneous admittivity: validation by simulation and tank experiment, Physiological measurement 30(10): 1087.

KAEWRAWANG, A., SWATDIPONPHALLOP S. AND SIRITARATIWAT, A. (2007), Study on complex permittivity of tropical Thai fruits, Journal of Applied Sciences 7(7): 1009-1012.

LEE, E., TS M.-E., SEO, J. K. AND WOO, E. J. (2012), Breast EIT using a new projected image reconstruction method with multi-frequency measurements, Physiological measurement 33(5): 751.

Nahvi, M. (2008), WIDEBAND ELECTRICAL IMPEDANCE SPECTRO-TOMOGRAPHIC IMAGING. School of Electronic and Electrical Engineering, The University of Leeds.

PACKHAM B., KOO H., ROMSAUEROVA A., AHN S., MCEWAN A., JUN S. AND HOLDER D. (2012), Comparison of frequency difference reconstruction algorithms for the detection of acute stroke using EIT in a realistic head-shaped tank, Physiological measurement 33(5): 767.

POLYDORIDES, N. (2002), Image reconstruction algorithms for soft-field tomography, University of Manchester: UMIST.

POLYDORIDES, N. AND LIONHEART, W. R. (2002), A Matlab toolkit for three-dimensional electrical impedance tomography: a contribution to the Electrical Impedance and Diffuse Optical Reconstruction Software project, Measurement Science and Technology 13(12): 1871.

RODGERS, T. AND KOWALSKI, A. (2010), An electrical resistance tomography method for determining mixing in batch addition with a level change, Chemical Engineering Research and Design 88(2): 204-212.

SEO, J. K., LEE J., KIM, S. W., ZRIBI, H. AND WOO, E. J. (2008), Frequency-difference electrical impedance tomography (fdEIT): algorithm development and feasibility study, Physiological measurement 29(8): 929.

SHARIFI, M., FATHY, M. AND MAHMOUDI, M. T. (2002), A classified and comparative study of edge detection algorithms. Information Technology: Coding and Computing, 2002. Proceedings. International Conference on, IEEE.

STANLEY, S., MANN, R. AND PRIMROSE, K. (2005), Interrogation of a precipitation reaction by electrical resistance tomography (ERT), AIChE journal 51(2): 607-614.

WANG, M., JIA X., BENNET, M. AND WILLIAMS, R. A. (2001), Electrical tomographic imaging for bubble column measurement and control. Intelligent Systems and Smart Manufacturing, International Society for Optics and Photonics.

WIAK, S., KRAWCZYK, A. AND DOLEZEL, I. (2008), Intelligent computer techniques in applied electromagnetics, Springer.

YANG, W. AND PENG, L. (2003), Image reconstruction algorithms for electrical capacitance tomography, Measurement Science and Technology 14(1): R1.

YANG, Y., JIA, J., POLYDORIDES, N. AND MCCANN, H. (2014), Effect of structured packing on EIT image reconstruction. Imaging Systems and Techniques (IST), 2014 IEEE International Conference on, IEEE.